

Ethanol steam reforming over $\text{Rh/Ce}_x\text{Zr}_{1-x}\text{O}_2$ catalysts: Impact of the $\text{CO-CO}_2\text{-CH}_4$ interconversion reactions on the H_2 production

Anne Birot^a, Florence Epron^{a,*}, Claude Descorme^b, Daniel Duprez^a

^a *Laboratoire de Catalyse en Chimie Organique (LACCO), UMR 6503 CNRS & University of Poitiers, 40 Avenue du Recteur Pineau, 86022 Poitiers Cedex, France*

^b *IRCELYON, UMR 5256 CNRS/Université Claude Bernard Lyon 1, 2 Avenue Albert Einstein, 69626 Villeurbanne Cedex, France*

Received 26 July 2007; received in revised form 1 October 2007; accepted 4 October 2007

Available online 7 October 2007

Abstract

$\text{Ce}_x\text{Zr}_{1-x}\text{O}_2$ mixed oxide-supported 1 wt.%Rh catalysts were prepared by wet impregnation using Rh nitrate as a precursor and calcined at 900 °C. They were characterized by BET surface area, XRD, CO_2 chemisorption and H_2 chemisorption at –85 °C and tested in the ethanol steam reforming at 600 °C under atmospheric pressure, with water to ethanol molar ratio equal to 4, without carrier gas. The best performances, i.e. the highest hydrogen yield and the lowest coke deposition, were obtained over $\text{Rh/Ce}_{0.5}\text{Zr}_{0.5}\text{O}_2$, i.e. 3.63 mol $\text{H}_2/\text{mol}_{\text{ethanol}}$. This catalyst was subsequently evaluated under various reaction conditions. Whatever the temperature and the water to ethanol ratio, the ethanol steam reforming yielded a large amount of methane, which tends to reduce the H_2 production. To elucidate the origin of the methane production, $\text{CO/CO}_2/\text{CH}_4$ interconversion reactions were studied. It was shown that such catalyst favours the formation of methane via CO hydrogenation. The direct hydrogenation of CO_2 was not observed. In parallel, the catalyst was active in the reverse water gas shift (RWGS) reaction between CO_2 and H_2 , leading CO and H_2O .

© 2007 Elsevier B.V. All rights reserved.

Keywords: Ethanol steam reforming; Rh/ceria–zirconia catalysts; CO and CO_2 hydrogenation; Water gas shift; Reverse water gas shift

1. Introduction

A rapid decrease of the fossil fuel resources has led most industrial countries to look for alternative energy sources or vectors such as hydrogen. For environmental reasons as well, the demand for hydrogen to run fuel cell-powered vehicles and small auxiliary power units (APU) should increase in the next 10 years. Today, hydrogen is produced on an industrial scale ($5 \times 10^{11} \text{ m}^3$ in 2000) by steam reforming (SR) of fossil fuels, mainly natural gas or naphtha [1]. SR reactors are connected to water gas shift units to increase the hydrogen yield. Virtually all carbon atoms are transformed into CO_2 , which is the main SR by-product. Since greenhouse gas emissions must be reduced, hydrogen should at least be partly produced from renewable resources such as ethanol, which can be obtained from biomass. The catalytic steam reforming of ethanol constitutes a promising route to the sustainable hydrogen production [2–6].

Steam reforming catalysts mainly consist of metals deposited on stable oxides. Rh is very active but Ni is preferred for practical applications. The specific role of the support was early recognized by Rostrup-Nielsen in the methane steam reforming reaction [7]. Grenoble [8] and Duprez [9,10] proposed a bifunctional mechanism for the steam reforming of hydrocarbons, especially aromatics. According to this mechanism, the water molecules are adsorbed on the support in the form of mobile hydroxyl groups and the hydrocarbon molecules are mainly activated on the metallic sites. A similar mechanism was proposed for the ethanol steam reforming. As a consequence, hydrophilic supports, with a high oxygen mobility, are expected to act as promoters in steam reforming reactions [8,11–13]. Furthermore, mobile oxygen species supplied by the support may participate in SR reactions and prevent the formation of coke on the metal particles [14]. However, several steps (dehydration to ethylene, dehydrogenation to acetaldehyde, condensation to acetone, cracking to C1 compounds) should be added to the hydrocarbon SR reaction mechanism since ethanol may react at both metallic and support sites [15–18].

* Corresponding author. Tel.: +33 5 49 45 48 32; fax: +33 5 49 45 34 99.

E-mail address: florence.epron.cognet@univ-poitiers.fr (F. Epron).

Ceria–zirconia mixed oxides have attracted a great attention as supports for Rh [19–22], Ni [23], Co and various metals [3,24] since they possess high oxygen mobility and tuneable surface properties (acid–base, redox). In the present work, the ethanol steam reforming reaction was studied over Rh catalysts supported on ceria–zirconia mixed oxides. Both the reaction temperature and the water to ethanol ratio R were varied in order to optimize the catalyst performances and selectivity.

Furthermore, significant amounts of methane were shown to form as a primary product upon the ethanol steam reforming reaction and, as far as the interconversion reactions between CO, CO₂ and H₂ might well be responsible for the formation of methane, these latter reactions were studied. Indeed, these reactions have been essentially studied up to now at temperatures lower than 350 °C [25–28]. Therefore, the last part of this paper will be devoted to the study of the interconversion reactions (CO + H₂ and CO₂ + H₂) at the ethanol steam reforming reaction temperature.

2. Experimental

2.1. Catalyst preparation

The Ce_xZr_{1-x}O₂ oxide supports ($x = 0, 0.50, 0.63, 0.68$ and 1) were directly supplied by Rhodia Electronics & Catalysis (La Rochelle, France) as ultra-thin powders. They were calcined beforehand for 6 h at 900 °C. Rh catalysts were prepared by wet impregnation of the supports with aqueous solutions of Rh nitrate to obtain 1 wt.% metal. Catalysts were dried at 120 °C for 24 h and subsequently calcined under flowing air (30 cm³/min) at 700 °C for 4 h.

2.2. Catalyst characterization

The structure of the Ce_xZr_{1-x}O₂ supports was determined by XRD using a Siemens D5005 diffractometer (Cu K α radiation, $\lambda = 1.5406$ Å). Crystalline phases were identified by comparison with ICDD files and the average crystallite size was derived using the Debye–Scherrer relation.

The BET surface area was measured by N₂ adsorption at –196 °C. Measurements were carried out in a Micromeritics flowsorb II apparatus.

CO₂ chemisorption measurements were carried out in a pulse chromatographic system [29]. The oxide sample (0.1 g) was first heated from room temperature to 450 °C (10 °C min⁻¹) under He and oxidized by O₂ pulses (0.25 cm³ pulse every other minute) until the saturation was reached. Then, the sample was cooled down to room temperature under He. Pulses of CO₂ (0.25 cm³ pulse every other minute) were injected until saturation.

The metallic phase dispersion was calculated from H₂ chemisorption experiments at low temperature (–85 °C) to limit “spillover” phenomenon [30]. A pulse chromatographic apparatus was used for such measurements. After reduction under hydrogen at 400 °C for 1 h and outgassing under flowing argon at the same temperature, the sample (0.15 g) was cooled down to RT under flowing argon. Then, the reactor was placed

in liquid nitrogen–acetone mixture to obtain the temperature of –85 °C. Afterwards, pulses of hydrogen were injected until saturation as indicated by the constant peak area of the last few pulses. As a result, the total hydrogen uptake (H_{C1}) was determined. Subsequently, the catalyst was flushed for 10 min under argon to remove the physically adsorbed hydrogen molecules. Finally, hydrogen was pulsed again until saturation (H_{C2}). The amount of chemisorbed hydrogen was derived as $H_C = H_{C1} - H_{C2}$.

2.3. Ethanol steam reforming

The ethanol steam reforming reaction was carried out in a fixed bed reactor ($L = 550$ mm, $\Phi_{\text{int}} = 12.5$ mm) made of refractory steel (TP310Z15CNS25). The catalyst (0.2 g), mixed together with carborundum (4.6 g), was placed in the middle of the reactor and pretreated under flowing H₂ (100 cm³ min⁻¹) for 1 h at 500 °C and atmospheric pressure.

After such a pretreatment, the temperature was increased to the reaction temperature under flowing H₂. Ethanol and water were introduced in the reactor via a HPLC pump. The ethanol flow rate was set at 0.098 mol h⁻¹ and the water flow rate was adjusted in order to obtain a water to ethanol molar ratio R equal to 4, 6 or 8. The weight hourly space velocity (WHSV) in gram of ethanol per gram of catalyst and per hour was equal to 22.54 h⁻¹ throughout this study. The mixture was preheated before entering the reactor. No carrier gas was fed to the system during the reaction.

The reaction temperature was checked using a thermocouple placed in the catalytic bed. Condensable vapours (ethanol, acetaldehyde, water, acetone, etc.) were trapped at +0.5 °C at the reactor outlet and further analyzed by HPLC equipped with an Aminex HPX-87H column, a refractometer and a UV diode array detector. Gas analysis was performed on line using a combination of three gas chromatographs, equipped with either TCD or FID detectors. The product distribution is given after 7 h of reaction.

The thermal decomposition of ethanol was studied under the same reaction conditions but in the absence of catalyst.

2.4. Hydrogenation of CO and CO₂

The CO and CO₂ hydrogenation reactions were performed in a fixed bed reactor. The catalyst (0.3 g) was pretreated under flowing H₂ (100 cm³/min) for 1 h at 500 °C and atmospheric pressure. The H₂:CO and H₂:CO₂ ratio were fixed at 4 in both cases. The reaction products were analyzed on line by TCD for H₂, CO, CO₂ and CH₄ and FID for the hydrocarbons.

2.5. Thermodynamic calculations

Gas compositions at equilibrium were obtained using a home-made program (THERMO). To run the calculations, the following inputs were required: (i) molar composition of the starting mixture, (ii) list of reactants and products. These calculations were based on (i) the minimization of the gas mixture Gibbs free energy and (ii) the mass conservation of the

different elements present in the mixture (C, O and H). Thermodynamic data were taken from [31] and interpolated at the appropriate temperature using the Clausius–Clapeyron equation. THERMO allows determining the equilibrium gas composition over large ranges of temperature and pressure. However, to avoid major deviations from ideality, it is more preferable to restrict the calculations to maximum 1000 °C and 100 bar.

3. Results and discussion

3.1. Catalyst characteristics

The XRD patterns of the three ceria–zirconia supports ($\text{Ce}_{0.68}\text{Zr}_{0.32}\text{O}_2$, $\text{Ce}_{0.63}\text{Zr}_{0.37}\text{O}_2$ and $\text{Ce}_{0.5}\text{Zr}_{0.5}\text{O}_2$) are reported in Fig. 1. The diffraction patterns of $\text{Ce}_{0.68}\text{Zr}_{0.32}\text{O}_2$ and $\text{Ce}_{0.63}\text{Zr}_{0.37}\text{O}_2$ are similar to that of cerium oxide, corresponding to the fluorite-type cubic structure. However, a shift of the lines to higher diffraction angles is observed, as reported in [19]. This shift is attributed to the lattice contraction upon the substitution of the Ce ions by the Zr ions. The $\text{Ce}_{0.5}\text{Zr}_{0.5}\text{O}_2$ support exclusively showed diffraction lines characteristic of the tetragonal structure. The support characteristics are summarized in Table 1. The crystallite size (L) of the supports was deduced from the full width at half-maximum (FWHM) of the corresponding diffraction peaks ($\Delta(2\theta)$) using the Debye–Scherrer formula. The geometrical surface area of these oxides could also be calculated from L , assuming the crystallites to be

spherical and using the density of the mixed oxide (ρ) approximated as follows:

$$\rho(\text{Ce}_x\text{Zr}_{1-x}\text{O}_2) = x'\rho(\text{CeO}_2) + (1 - x')\rho(\text{ZrO}_2) \quad (1)$$

where x' is the weight loading of CeO_2 in the mixed oxide (i.e. $x' = 0.75$ for $\text{Ce}_{0.68}\text{Zr}_{0.32}\text{O}_2$).

The support characteristics are in accordance with those reported in [32]. The BET surface area is roughly the same for the three supports, ca. $45 \text{ m}^2 \text{ g}^{-1}$. However, it should be noticed that the surface areas calculated from the XRD patterns are higher than the measured BET surface areas, whatever the composition of the mixed oxide. This observation indicates that the oxide grains are polycrystalline, with grain boundaries which are not accessible to the gases. The lowest crystallite size is obtained with the support with the highest zirconium loading ($\text{Ce}_{0.50}\text{Zr}_{0.50}\text{O}_2$), which is also the only support with a tetragonal structure.

The three supports were also characterized by CO_2 chemisorption in order to estimate the basic site density. The corresponding CO_2 chemisorption results, as well as the BET surface areas of all supports, including CeO_2 and ZrO_2 for comparison purposes, are reported in Table 2. The BET surface areas of the mixed oxides are higher than those of the pure oxides. Furthermore, since the amount of chemisorbed CO_2 is an indication of the basicity, the supports can be classified in order of increasing basicity as follows:

$$\text{ZrO}_2 < \text{CeO}_2 < \text{Ce}_{0.68}\text{Zr}_{0.32}\text{O}_2 \sim \text{Ce}_{0.63}\text{Zr}_{0.37}\text{O}_2 < \text{Ce}_{0.50}\text{Zr}_{0.50}\text{O}_2$$

Mixed oxides are more basic than ceria and zirconia and $\text{Ce}_{0.50}\text{Zr}_{0.50}\text{O}_2$ is the most basic support among the mixed oxides. This is in agreement with the results of Cutrufello et al. [33]. However, these authors observed slightly higher basicities for the mixed oxides they used. The total number of basic sites was equal to $\sim 2.6 \mu\text{mol m}^{-2}$ for $\text{Ce}_{0.8}\text{Zr}_{0.2}\text{O}_2$ and to $\sim 2.4 \mu\text{mol m}^{-2}$ for $\text{Ce}_{0.5}\text{Zr}_{0.5}\text{O}_2$.

The catalyst characteristics are summarized in Table 3. The metal dispersion was calculated from H_2 chemisorption measurements, assuming a stoichiometry H/Rh_5 equal to 1. Furthermore, the rhodium particle size was calculated from the dispersion D (in %), considering the particles to be cubic, with one face in contact with the support and assuming an equidistribution of the (1 0 0), (1 1 0) and (1 1 1) faces. Thus, the particle size d (in nm) is given by

$$d = \frac{91}{D} \quad (2)$$

The results reported in Table 3 show that the $\text{Rh}/\text{Ce}_{0.50}\text{Zr}_{0.50}\text{O}_2$ catalyst presents the best metal dispersion.

3.2. Ethanol steam reforming

3.2.1. Effect of the support

All three catalysts were evaluated in the ethanol steam reforming reaction at 600 °C and atmospheric pressure, with water to ethanol molar ratio (R) equal to 4. The product

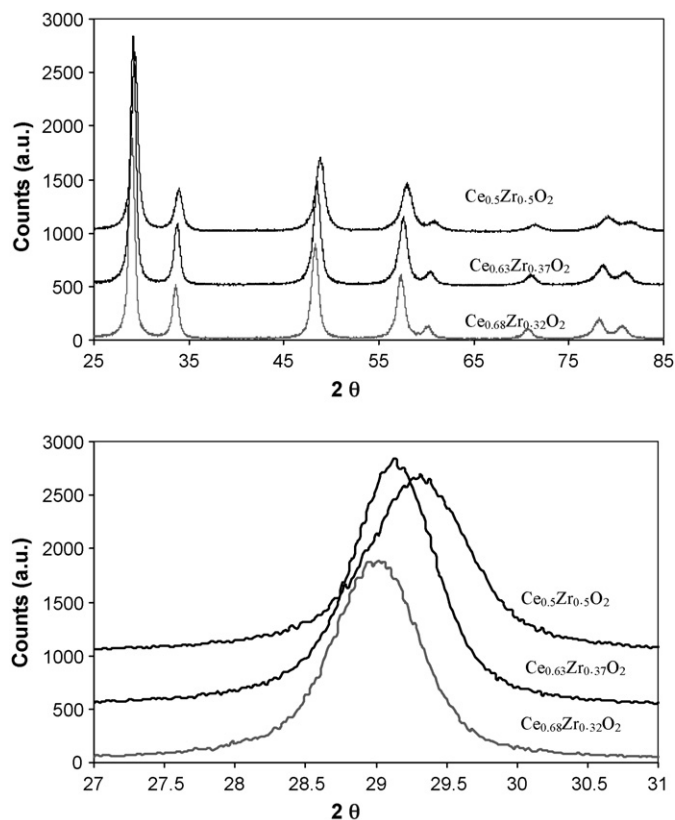


Fig. 1. XRD patterns of the three $\text{Ce}_{0.68}\text{Zr}_{0.32}\text{O}_2$, $\text{Ce}_{0.63}\text{Zr}_{0.37}\text{O}_2$ and $\text{Ce}_{0.5}\text{Zr}_{0.5}\text{O}_2$ ceria–zirconia supports.

Table 1
Structural and textural characteristics of the $\text{Ce}_x\text{Zr}_{1-x}\text{O}_2$ supports

Support	BET surface area ($\text{m}^2 \text{g}^{-1}$)	ICDD files	Crystalline structure	Lattice parameter ^a (Å)	Crystallites size ^a (Å)	Surface area ^a ($\text{m}^2 \text{g}^{-1}$)
$\text{Ce}_{0.68}\text{Zr}_{0.32}\text{O}_2$	45	28–0271 38–1439	Cubic	$a = 5.331$	116	81
$\text{Ce}_{0.63}\text{Zr}_{0.37}\text{O}_2$	43	38–1439	Cubic	$a = 5.314$	118	75
$\text{Ce}_{0.50}\text{Zr}_{0.50}\text{O}_2$	45	38–1436	Tetragonal	$a = b = 3.725$ $c = 5.269$	100	90

^a Calculated from the XRD patterns.

Table 2
Estimation of the support basicity from CO_2 chemisorption measurements

Catalyst	Surface area ($\text{m}^2 \text{g}^{-1}$)	CO_2 chemisorbed ($\mu\text{mol CO}_2 \text{m}^{-2}$)
CeO_2	23	1.5
$\text{Ce}_{0.68}\text{Zr}_{0.32}\text{O}_2$	45	1.8
$\text{Ce}_{0.63}\text{Zr}_{0.37}\text{O}_2$	43	1.8
$\text{Ce}_{0.50}\text{Zr}_{0.50}\text{O}_2$	45	2.0
ZrO_2	35	1.0

Table 3
BET surface area, metal dispersion and metal particle size of the 1%Rh/ $\text{Ce}_x\text{Zr}_{1-x}\text{O}_2$ catalysts

Catalyst	Surface area ($\text{m}^2 \text{g}^{-1}$)	Metal dispersion (%)	Metal particle size (nm)
1%Rh/ $\text{Ce}_{0.68}\text{Zr}_{0.32}\text{O}_2$	46	47	2.0
1%Rh/ $\text{Ce}_{0.63}\text{Zr}_{0.37}\text{O}_2$	42	49	1.9
1%Rh/ $\text{Ce}_{0.50}\text{Zr}_{0.50}\text{O}_2$	44	60	1.5

distribution as well as the carbon mass balance are reported in Table 4 and compared to the product distribution at equilibrium. The carbon mass balance might be used as an indication for the deposition of coke during the reaction. Indeed, the lowest the carbon mass balance, the highest the coke deposition. This relationship was confirmed by performing *in situ* temperature programmed oxidation (TPO) immediately after the steam reforming reaction, once all reaction lines were purged. The amount of CO_2 produced under flowing air (TPO) corresponded exactly to the amount of carbon which was missing to complete the balance. It is noteworthy that TPO experiments performed on the catalyst alone, recovered after the reaction, showed that only a small fraction of the coke is deposited on the catalyst while the main part is deposited on the reactor walls. The blank experiment performed in the same reaction conditions shows

that only 18% of ethanol is converted in the absence of catalyst probably by ethanol thermal decomposition and the same result was obtained in a quartz reactor. The distribution of products cannot be attributed to the ethanol steam reforming reaction, water being produced and not consumed. The production of water can be explained by ethanol dehydration yielding ethylene that is a coke precursor. Ethanol dehydrogenation yielding acetaldehyde also occurs. In the absence of catalyst, the amount of coke, deduced from carbon mass balance is higher than that observed in the presence of catalyst. Then it can be inferred that (i) the presence of the catalyst limits the formation of coke and (ii) the coke produced during the reaction in the presence of catalyst and deposited on the reactor walls is due to the thermal decomposition of ethanol, which occurs in the reactor before having reached the catalyst bed.

The product distribution obtained in the presence of catalyst, especially the amount of CO , CO_2 and CH_4 produced, is very similar for all catalysts. The rhodium is not a very good metal for the water gas shift reaction [34] but ceria strongly improves its performances [35–37]. Diagne et al. [19] demonstrated that the use of ceria–zirconia instead of pure CeO_2 decreases the amount of CO produced during ethanol steam reforming in the presence of Rh/ CeO_2 – ZrO_2 . The results presented in Table 4 are in accordance with those reported in [19]. Accordingly, the values of the CO_2/CO molar ratio obtained with the various catalysts are very high, even higher than the ratio calculated from the thermodynamical values. This may be explained by the concomitance of two phenomena: (i) a high activity of this type of catalyst for the water gas shift reaction and (ii) the occurrence of another reaction consuming CO . As the quantities of CO_2 and H_2 produced are also lower than the values predicted by the thermodynamics whereas the amount of methane is higher, the low amount of CO may also be explained by the methanation reaction of CO by H_2 . This point will be addressed in the next paragraph. No acetaldehyde was

Table 4
Ethanol steam reforming at $T = 600^\circ\text{C}$ and atmospheric pressure with R (water/ethanol) = 4 over 1%Rh/ $\text{Ce}_x\text{Zr}_{1-x}\text{O}_2$ catalysts

Catalyst	Products ($\text{mol/mol}_{\text{ethanol}}$)								CO_2/CO molar ratio	Carbon mass balance (%)	Ethanol conversion (%)
	H_2O	H_2	CO_2	CO	CH_4	C_2H_4	C_2H_6	CH_3CHO			
Equilibrium composition	<i>2.41</i>	<i>3.78</i>	<i>0.98</i>	<i>0.61</i>	<i>0.39</i>	<i>0</i>	<i>0</i>	<i>0</i>	<i>1.6</i>	100	100
Blank	4.15	0.029	0.02	0.008	0.003	0.008	0	0.017	0.4	86	18
Rh/ $\text{Ce}_{0.68}\text{Zr}_{0.32}\text{O}_2$	2.6	3.47	0.89	0.41	0.45	0.003	0.003	0	2.17	88	99
Rh/ $\text{Ce}_{0.63}\text{Zr}_{0.37}\text{O}_2$	2.62	3.44	0.94	0.41	0.46	0.003	0.004	0	2.29	91	99
Rh/ $\text{Ce}_{0.50}\text{Zr}_{0.50}\text{O}_2$	2.36	3.63	0.92	0.44	0.50	0	0.004	0	2.07	93	99.9

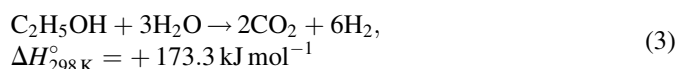
Italic indicates values at the equilibrium.

observed, whatever the catalyst. Even though acetaldehyde had clearly been identified as an intermediate product in earlier works, it is very likely to be rapidly transformed under the reaction conditions we applied. However it was verified that acetaldehyde is formed in the course of the reaction in the presence of our Rh/CeO₂–ZrO₂ catalysts by decreasing the contact time. Acetaldehyde can undergo decarbonylation to produce methane and carbon monoxide but Rh/CeO₂–ZrO₂ catalysts are more likely to favour the steam reforming reaction yielding carbon dioxide and hydrogen, as it was proposed in [22]. The highest hydrogen yield was obtained with Rh/Ce_{0.50}Zr_{0.50}O₂, i.e. when the cerium content is the lowest. Moreover, ethylene, as an intermediate, was not observed to form on this catalyst. In parallel, the highest carbon mass balance was observed on this catalyst, indicating the lowest coke deposition level. As a result, the deactivation was less pronounced for this catalyst. This result could be explained by the higher basicity of the Ce_{0.50}Zr_{0.50}O₂ support compared to the other supports. Indeed, basicity might help not only to prevent the formation of coke but also to favour the steam reforming reaction since the OH group mobility is improved on basic supports [11]. Such trends as a function of the cerium content, both in terms of hydrogen yield and stability, are just opposite to what was observed by Roh et al. on 2%Rh/Ce_xZr_{1-x}O₂ catalysts at 450 °C [38]. However, it is difficult to compare since the reaction temperature was different, as well as the metal content.

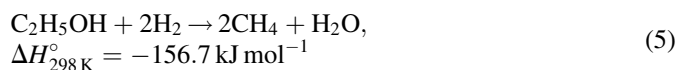
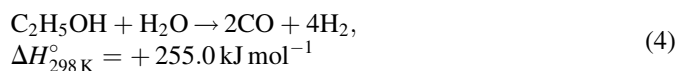
In the following, the effect of the reaction conditions on the Rh/Ce_{0.50}Zr_{0.50}O₂ catalyst performances will be examined.

3.2.2. Effect of the reaction conditions

To reach the highest hydrogen yield, the impact of various reaction parameters (temperature and water to ethanol ratio) on the ethanol steam reforming reaction was studied. The overall reaction leading to the maximum hydrogen production is the ethanol steam reforming reaction to CO₂ and H₂ (Eq. (3)). Indeed, 6 mol H₂/mol_{ethanol} or 3 mol H₂/mol CO₂ is produced through the following reaction.



However, many other gases, especially CO and CH₄, are produced upon reaction. Such by-products tend to decrease the H₂ yield: only 4 mol H₂/mol_{ethanol} (i.e. 2 mol H₂/mol CO) is produced upon reaction (4). Furthermore, the formation of methane through reaction (5) consumes 2 mol H₂/mol_{ethanol} or 1 mol H₂/mol CH₄.

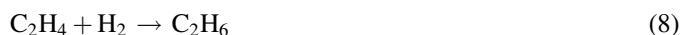


Intermediate products, such as acetaldehyde, resulting from the ethanol dehydrogenation reaction, or ethylene, produced by dehydration, are also produced according to the following

equations:



Furthermore, acetaldehyde rapidly decomposes to CH₄ and CO [5] and ethane is produced from the hydrogenation of ethylene



3.2.2.1. Reaction temperature. The catalytic performances of Rh/Ce_{0.50}Zr_{0.50}O₂ were first evaluated at different temperatures, between 500 and 600 °C at atmospheric pressure with *R* = 4.

The evolution of the dry gas flow rate is presented in Fig. 2 as a function of time on stream. For reactions performed at 500 and 550 °C, the total gas flow rate decreases as the function of time, indicating that the catalyst deactivates, which is not the case for the reaction performed at higher temperature (600 °C). This observation is in accordance with the values of the carbon mass balance reported in Table 5 indicating that the carbon production increases when the reaction temperature decreases. The results reported in Table 5 also show that the production of hydrogen increases with temperature. The highest yield in H₂ is obtained at 600 °C over 1%Rh/Ce_{0.50}Zr_{0.50}O₂ (3.63 mol H₂/mol_{ethanol}), as predicted by the thermodynamics.

For temperatures lower than 600 °C, the amount of water at the outlet is exactly equal to the amount of water introduced at the reactor inlet. Two possibilities: (i) water does not react at all with ethanol or (ii) water is simultaneously consumed and produced during the ethanol SR. Ethylene is observed for reactions performed at 500 and 550 °C, but not at 600 °C (Table 5). Then, it is proposed that water could originate from the ethanol dehydration reaction [4–6], yielding ethylene, which is an undesired product since it is a precursor of coke and leads to deactivation [2]. The formation of coke at the lowest temperature is confirmed by the low carbon mass balance. Furthermore, it is in agreement with the evolution of the dry gas

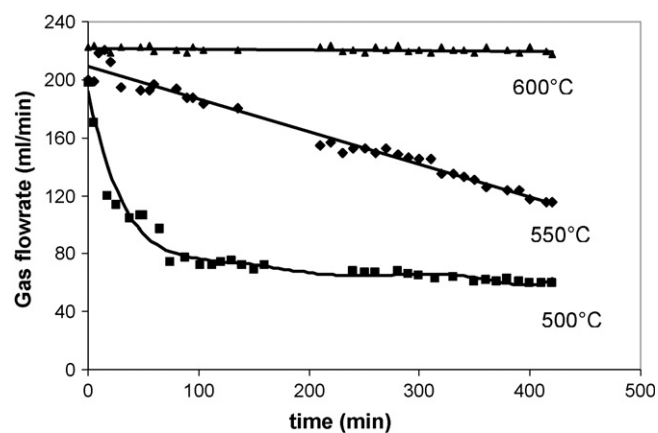


Fig. 2. Evolution of the gas flow rate vs. time on stream upon ethanol steam reforming over 1%Rh/Ce_{0.5}Zr_{0.5}O₂ catalyst (*P* = 1 bar, *T* = 500, 550 and 600 °C, *R* = 4).

Table 5

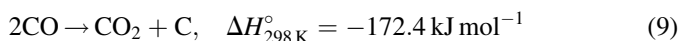
Ethanol steam reforming of ethanol over 1%Rh/Ce_{0.50}Zr_{0.50}O₂ at 500, 550 and 600 °C with $R = 4$ at atmospheric pressure: yield in different products, equilibrium constant of methane steam reforming reaction (K_{MSR}), mass action ratio (MAR_{MSR}) and shift from the equilibrium x , obtained at the different temperatures

Catalyst	T (°C)	Products (mol/mol _{ethanol})							Carbon mass balance (%)	Ethanol conversion (%)	K_{MSR} (bar ²)	MAR (bar ²)	x (mol/mol _{ethanol})
		H ₂ O	H ₂	CO ₂	CO	CH ₄	C ₂ H ₄	C ₂ H ₆					
Equilibrium composition	500	<i>2.99</i>	<i>2.15</i>	<i>0.93</i>	<i>0.14</i>	<i>0.93</i>	<i>0</i>	<i>0</i>		100	0.010		
Rh/Ce _{0.50} Zr _{0.50} O ₂	500	4.00	1.56	0.33	0.21	0.21	0.025	0.003	46	98.7		0.024	0.09
Equilibrium composition	550	<i>2.68</i>	<i>2.96</i>	<i>1.00</i>	<i>0.32</i>	<i>0.68</i>	<i>0</i>	<i>0</i>		100	0.078		
Rh/Ce _{0.50} Zr _{0.50} O ₂	550	4.00	1.85	0.44	0.27	0.28	0.015	0.005	57	98.5		0.033	−0.11
Equilibrium composition	600	<i>2.41</i>	<i>3.78</i>	<i>0.98</i>	<i>0.61</i>	<i>0.39</i>	<i>0</i>	<i>0</i>		100	0.525		
Rh/Ce _{0.50} Zr _{0.50} O ₂	600	2.36	3.63	0.91	0.44	0.50	0	0.004	93	99.9		0.290	−0.09

Italic indicates values at the equilibrium.

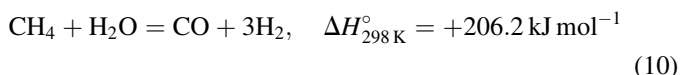
flow rate as a function of time for the three temperatures (Fig. 2).

Another possible route to the production of coke could be the CO disproportionation reaction, also known as the Boudouard reaction



The occurrence of this reaction will be examined in Section 3.3.

At 600 °C the distribution in water and CO₂ is very close to the equilibrium composition, contrary to what is observed at 500 and 550 °C. However, the amount of CH₄ that is produced (0.50 mol CH₄/mol_{ethanol}) is higher than the thermodynamic equilibrium data (0.39 mol CH₄/mol_{ethanol}), whereas the amounts of H₂ and CO are lower. This result can be explained by the poor activity of the catalyst for the methane steam reforming reaction (reaction (10)).



To evaluate the excess of methane due to the poor activity of the catalyst for this reaction, we have calculated the equilibrium constants at the different temperatures K_{MSR} and compared them with the experimental mass action ratios (MAR) calculated according to [39,40]. Results are reported in Table 5.

Let us consider the equilibrium constant

$$K_{\text{MSR}} = \frac{p_{\text{CO}} p_{\text{H}_2}^3}{p_{\text{CH}_4} p_{\text{H}_2\text{O}}} = \frac{\text{C OH}_2^3}{\Sigma^2 \text{CH}_4 \text{H}_2\text{O}}$$

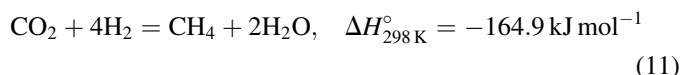
where p is the partial pressure of the different products as calculated at the equilibrium composition, CO, H₂, CH₄ and

H₂O represent the molar yield of the different products at the equilibrium and Σ is the sum of molar yields of the whole products. It is possible to calculate the shift from the equilibrium x considering that the mass action ratio MAR calculated from the experimental values corresponds to

$$\text{MAR} = \frac{(\text{CO} + x)(\text{H}_2 + 3x)^3}{(\Sigma + 2x)^2(\text{CH}_4 - x)(\text{H}_2\text{O} - x)}$$

The results reported in Table 5 show that except for the reaction performed at 500 °C, K_{MSR} is much higher than the MAR, indicating that the experiment leads to an excess of CH₄ and less CO and H₂ compared to the equilibrium values. The shift x from the equilibrium is around −0.1 mol per mole of ethanol introduced.

As methane is not converted at 600 °C in the presence of the 1%Rh/Ce_{0.50}Zr_{0.50}O₂ catalyst it may be interesting to study the CO methanation reaction that is the inverse of reaction (10) and also the CO₂ methanation reaction, according to reaction (11), which is also possible



CO and CO₂ methanation will be studied in Section 3.3.

3.2.2.2. Water to ethanol ratio. The effect of the water to ethanol ratio (R) on the catalytic performances of 1%Rh/Ce_{0.50}Zr_{0.50}O₂ was evaluated at 600 °C at atmospheric pressure for $R = 4, 6$ and 8 . Indeed, it has been reported in the literature [2] that the hydrogen production is favoured when the water to ethanol ratio is greater than 2, while the CO and CH₄ yields are

Table 6

Ethanol steam reforming over 1%Rh/Ce_{0.50}Zr_{0.50}O₂ at 600 °C and atmospheric pressure for $R = 4, 6$ or 8 : yield in different products, equilibrium constant of methane steam reforming reaction (K_{MSR}), mass action ratio (MAR) and shift from the equilibrium x , obtained at different water to ethanol ratio

Catalyst	Ratio	Products (mol/mol _{ethanol})							Carbon mass balance (%)	Ethanol conversion (%)	K_{MSR} (bar ²)	MAR (bar ²)	x (mol/mol _{ethanol})
		H ₂ O	H ₂	CO ₂	CO	CH ₄	C ₂ H ₄	C ₂ H ₆					
Equilibrium composition	4	<i>2.41</i>	<i>3.78</i>	<i>0.98</i>	<i>0.61</i>	<i>0.39</i>	<i>0</i>	<i>0</i>	–	100	0.525		
Rh/Ce _{0.50} Zr _{0.50} O ₂	4	2.36	3.63	0.91	0.44	0.50	0	0.004	93.3	99.9		0.290	−0.09
Equilibrium composition	6	<i>4.00</i>	<i>4.55</i>	<i>1.23</i>	<i>0.55</i>	<i>0.23</i>	<i>0</i>	<i>0</i>	–	100	0.505		
Rh/Ce _{0.50} Zr _{0.50} O ₂	6	4.40	3.53	1.09	0.41	0.46	0	0	98.0	99.4		0.091	−0.23
Equilibrium composition	8	<i>5.73</i>	<i>5.01</i>	<i>1.39</i>	<i>0.48</i>	<i>0.13</i>	<i>0</i>	<i>0</i>	–	100	0.499		
Rh/Ce _{0.50} Zr _{0.50} O ₂	8	6.60	3.20	1.08	0.21	0.38	0	0	98.4	99.3		0.021	−0.34

Italic indicates values at the equilibrium.

lowered. Furthermore, high water concentrations were shown to inhibit the formation of coke.

The results reported in Table 6 show that the selectivity towards H_2 is roughly the same whatever the water to ethanol ratio (4, 6 or 8). However, the selectivity values fall below the equilibrium data, especially for $R = 8$. Moreover, the catalyst is obviously more stable at $R = 8$ since the carbon mass balance is as high as 98.4%. Finally, for $R = 8$, (i) the amount of water (6.6 mol/mol_{ethanol}) is also above the thermodynamic data (5.73 mol/mol_{ethanol}) and (ii) the formation of CH_4 is largely favoured since the amount of methane is about three times higher than the value predicted by thermodynamics. One possible reaction to explain the formation of extra water and methane could be the ethanol hydrogenolysis (Eq. (5)). However, CH_4 could also be produced by steam reforming of ethane, ethylene or acetaldehyde, or from the CO or CO_2 hydrogenation reactions.

3.3. CO and CO_2 hydrogenation

It was shown above that, when the ethanol SR is performed in the presence of 1%Rh/Ce_{0.50}Zr_{0.50}O₂ at 600 °C under atmospheric pressure, the undesired production of methane exceeds the value predicted by the thermodynamics. Consequently, different reactions leading to the production of methane must be kinetically favoured over the reactions involving the conversion of methane. In order to study the possible pathways to the formation of methane, interconversion reactions between the different gases were studied, especially the hydrogenation of CO and CO_2 , also named as “methanation” reactions. These hydrogenation reactions have been extensively studied in a number of papers since the first report of Sabatier at the beginning of the 20th century [25,41–45]. The most studied catalysts were based on nickel. However, noble metals such as rhodium were also shown to be active in the CO and CO_2 hydrogenation reactions. The catalyst performances were further shown to be very sensitive to the support [26,27].

According to the literature and Eqs. (10) and (11), the main product in the CO or CO_2 hydrogenation is methane. Mills and Steffen [41] demonstrated that reaction (11) does not occur in the presence of carbon monoxide. Finally, CO hydrogenation could also lead to both methane and carbon dioxide

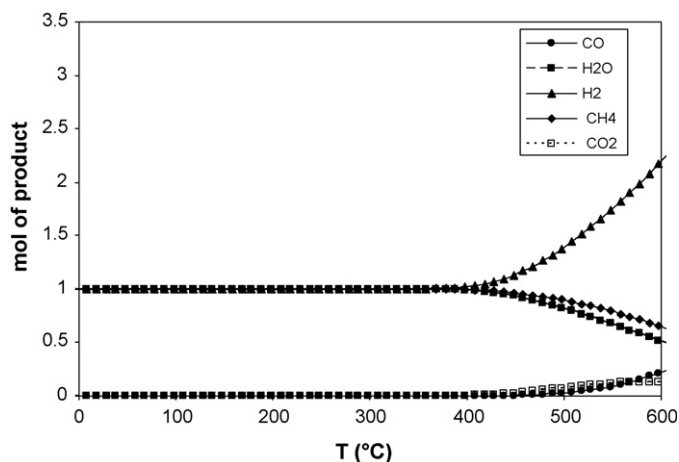
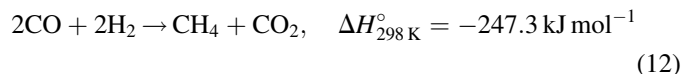
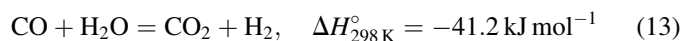


Fig. 3. Effect of temperature on the reaction product distribution as calculated from the thermodynamic data upon CO hydrogenation at atmospheric pressure with $H_2/CO = 4$.

In fact, reaction (12) is a combination of reaction (10) and the water gas shift (WGS) reaction (13)



3.3.1.1. CO hydrogenation

The CO methanation was studied at three different temperatures, namely 400, 500 and 600 °C. The results reported in Table 7 are compared with the thermodynamic equilibrium data, considering that reactions (10) and (13) could occur with the formation of water, methane and carbon dioxide. These reactions are exothermic and disfavoured at high temperature. The evolution of the different products as a function of temperature is presented in Fig. 3. According to the thermodynamics, the conversion of CO is complete before ca. 420 °C. For this reason, most of the studies reported in the literatures dealing with the CO hydrogenation were carried out at temperatures below 400 °C, essentially between 150 and 350 °C [25–28]. In this temperature range, thermodynamics predicts that CO is completely hydrogenated into methane with the formation of water. CO_2 is only produced at temperatures higher than ≈ 340 °C. Above 420 °C, the CO conversion decreases continuously with temperature. Then, it is difficult to compare the present results obtained between 400 and 600 °C with those reported in the literature.

Table 7

CO hydrogenation at 400, 500 and, 600 °C at atmospheric pressure with $H_2/CO = 4$ over 1%Rh/Ce_{0.50}Zr_{0.50}O₂

	<i>T</i> (°C)	Products (mol/mol CO)					Mass balance (%)		
		<i>H</i> ₂	CO	CO ₂	CH ₄	H ₂ O	C	O	H
Equilibrium composition	400	<i>1.02</i>	<i>0</i>	<i>0.006</i>	<i>0.99</i>	<i>0.99</i>	–	–	–
Rh/Ce _{0.50} Zr _{0.50} O ₂	400	2.10	0.09	0.14	0.58	0.74	81	111	100
Equilibrium composition	500	<i>1.39</i>	<i>0.03</i>	<i>0.07</i>	<i>0.89</i>	<i>0.82</i>	–	–	–
Rh/Ce _{0.50} Zr _{0.50} O ₂	500	2.31	0.14	0.12	0.53	0.63	79	100	100
Equilibrium composition	600	<i>2.19</i>	<i>0.22</i>	<i>0.13</i>	<i>0.65</i>	<i>0.52</i>	–	–	–
Rh/Ce _{0.50} Zr _{0.50} O ₂	600	3.27	0.64	0.08	0.26	0.2	98	100	100

Italic indicates values at the equilibrium.

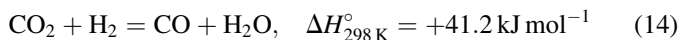
Experimentally, the CO conversion over 1%Rh/Ce_{0.50}Zr_{0.50}O₂ followed the trends predicted by thermodynamics. The amount of unconverted CO increased with temperature. Still, the CO conversion was lower than the thermodynamic values. Such an observation tends to indicate that the CO hydrogenation is kinetically limited over the 1%Rh/Ce_{0.50}Zr_{0.50}O₂ catalyst. In the same way, whatever the reaction temperature, the amount of methane actually produced is below the equilibrium values. Such a low yield in methane, in addition to the high amount of unreacted hydrogen, is a direct consequence of the poor CO conversion.

In a similar way, the amount of carbon dioxide should increase when the temperature increases from 400 to 600 °C (Fig. 3). In fact, the amount of CO₂ experimentally produced showed the opposite trend: the amount of CO₂ decreased when the reaction temperature increased. If one refers to the carbon mass balance, the best experimental value is obtained at 600 °C (98%), when the CO₂ production is the lowest. For temperatures lower than 600 °C, the amount of CO₂ produced is high and the carbon mass balance deteriorates, indicating the possible deposition of coke. Then, it can be inferred that the production of CO₂ could also derive from the CO disproportionation (“Boudouard” reaction) and not only from the CO hydrogenation reaction.

In conclusion, 1%Rh/Ce_{0.50}Zr_{0.50}O₂ is able to hydrogenate CO, principally to methane and water, even though this reaction is somehow kinetically limited. The formation of CO₂ is also observed, together with the formation of coke. Both CO₂ and coke productions would mainly result from the CO disproportionation reaction.

3.3.1.2. Hydrogenation of CO₂

CO₂ methanation was studied at two different temperatures, namely 500 and 600 °C. The results reported in Table 8 are compared to the equilibrium data, considering that CO₂ hydrogenation occurs according to reaction (11). Reaction (11) is in fact a combination between (i) the reaction of CO methanation (inverse of reaction (10)), which is exothermic and leads to methane and water and (ii) the reverse water gas shift reaction (14), which is in turn endothermic and leads to carbon monoxide and water



The evolution of the different reaction products as a function of temperature at equilibrium is presented in Fig. 4. The

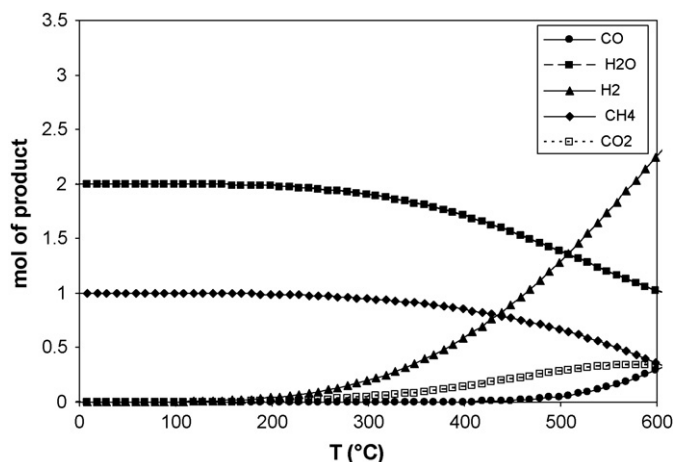


Fig. 4. Effect of temperature on the reaction product distribution as calculated from the thermodynamic data upon CO₂ hydrogenation at atmospheric pressure with H₂/CO₂ = 4.

complete conversion of CO₂ is only observed at temperatures below ca. 150 °C. Above this temperature, the CO₂ conversion decreases as the temperature increases. Up to ca. 350 °C, the only reaction products are methane and water, according to reaction (11). The amount of CO produced through the reverse WGS reaction only becomes significant around 450 °C. At 600 °C, virtually the same amounts of methane and carbon monoxide are produced. Classically, the hydrogenation of CO₂, as reported in the literatures, is performed at temperatures below 320 °C, when the only product is methane [26,27,46,47]. However, Iizuka et al. [26] also observed that a small amount of CO is formed along with methane from 200 °C upon reaction over a Rh/ZrO₂ catalyst. Furthermore, Kusama et al. [48] showed that even at temperatures as low as 200 °C, CO is the main product when 1%Rh/SiO₂ is used as a catalyst. These authors demonstrated that the product selectivity strongly depends on the metal loading that is the Rh particle concentration at the support surface. Methane was preferentially produced on 10%Rh/SiO₂. This difference in selectivity was explained by the fact that CO, which is produced in both cases from the CO₂ hydrogenation, can either (i) desorb as CO or (ii) hydrogenate to methane. The latter reaction would be favoured on the largest Rh particles, when adsorbed CO and hydrogen molecules may co-exist.

Experimental results presented in Table 8 show that the trends are different from the thermodynamic data. Indeed, the conversion of CO₂ is greater at 600 °C than at 500 °C and the

Table 8
CO₂ hydrogenation at 500 and 600 °C under atmospheric pressure with H₂/CO₂ = 4 over 1%Rh/Ce_{0.50}Zr_{0.50}O₂

	<i>T</i> (°C)	Products (mol/mol CO ₂)					Mass balance (%)		
		H ₂	CO ₂	CO	CH ₄	H ₂ O	C	O	H
Equilibrium composition	500	<i>1.30</i>	<i>0.28</i>	<i>0.05</i>	<i>0.66</i>	<i>1.38</i>	–	–	–
Rh/Ce _{0.50} Zr _{0.50} O ₂	500	3.16	0.41	0.40	0.08	0.78	89	100	102
Equilibrium composition	600	<i>2.26</i>	<i>0.34</i>	<i>0.30</i>	<i>0.36</i>	<i>1.02</i>	–	–	–
Rh/Ce _{0.50} Zr _{0.50} O ₂	600	3.10	0.36	0.30	0	0.98	66	100	102

Italic indicates values at the equilibrium.

amount of methane which is formed is negligible at both temperatures. The only reaction products are carbon monoxide and water. Then, it can be inferred that the only reaction which is kinetically favoured in the presence of 1%Rh/Ce_{0.50}Zr_{0.50}O₂, under the applied reaction conditions, is the reverse water gas shift reaction. The formation of methane is completely disfavoured. As far as the carbon mass balance is concerned, it can be seen from Table 8 that the value is far from 100%, whatever the temperature. This result can be explained by the formation of coke according to the Boudouard reaction, which probably leads to the deactivation of the catalyst. This type of deactivation during the reverse water gas shift reaction is well-known, especially over Pt-based catalysts [49].

4. Summary

In summary, 1 wt.%Rh/Ce_xZr_{1-x}O₂ catalysts were prepared by wet impregnation, using Rh nitrate as a precursor, and characterized by BET surface area, XRD, CO₂ chemisorption and H₂ chemisorption at –85 °C. The best metal dispersion, ca. 60%, was obtained on the support with the lowest cerium content. Ce_xZr_{1-x}O₂ mixed oxide supports appeared to be highly basic, as evidenced by CO₂ chemisorption. Three catalysts were tested in the ethanol steam reforming at 600 °C under atmospheric pressure, with water to ethanol molar ratio equal to 4. The best performances, i.e. the highest hydrogen yield and the lowest coke deposition, were obtained over Rh/Ce_{0.5}Zr_{0.5}O₂. This catalyst was then tested under various reaction conditions. Whatever the temperature and the water to ethanol ratio, the ethanol steam reforming reaction yielded a large amount of methane. As far as the formation of methane is detrimental to the H₂ production, CO/CO₂/CH₄ interconversion reactions were also studied in order to evidence the possible routes to CH₄, especially the CO and CO₂ hydrogenation reactions. It was shown that 1 wt.%Rh/Ce_{0.5}Zr_{0.5}O₂ could favour the formation of CH₄ through the CO hydrogenation reaction while the reverse water gas shift (RWGS) reaction led to CO and H₂O when CO₂ and H₂ were fed over such catalyst.

References

- [1] J.R. Rostrup-Nielsen, in: J.R. Anderson, M. Boudart (Eds.), *Catalysis, Science and Technology*, vol. 5, Springer, Berlin, 1984, p. 1.
- [2] E.Y. Garcia, M.A. Laborde, *Int. J. Hydrogen Energy* 16 (1991) 307.
- [3] F. Aupretre, C. Descorme, D. Duprez, *Catal. Commun.* 3 (2002) 263.
- [4] D.K. Liguras, D.I. Kondarides, X.E. Verykios, *Appl. Catal. B* 43 (2003) 345.
- [5] A.N. Fatsikostas, X.E. Verykios, *J. Catal.* 225 (2004) 439.
- [6] F. Aupretre, C. Descorme, D. Duprez, D. Casanave, D. Uzio, *J. Catal.* 233 (2005) 464.
- [7] J.R. Rostrup-Nielsen, *J. Catal.* 31 (1973) 173.
- [8] D.C. Grenoble, *J. Catal.* 51 (1978) 212.
- [9] D. Duprez, P. Pereira, A. Miloudi, R. Maurel, *J. Catal.* 75 (1982) 151.
- [10] D. Duprez, *Appl. Catal. A* 82 (1992) 111.
- [11] D. Duprez, *Catal. Today* 112 (2006) 17.
- [12] K. Polychronopoulou, A.M. Efstathiou, *Catal. Today* 116 (2006) 341.
- [13] L.S.F. Feio, C.E. Hori, S. Damyanova, F.B. Noronha, W.H. Cassinelli, C.M.P. Marques, J.M.C. Bueno, *Appl. Catal. A* 316 (2007) 107.
- [14] Y. Wang, Y.H. Chin, R.T. Rozmiarek, B.R. Johnson, Y. Gao, J. Watson, A.Y.L. Tonkovich, D.P. Van der Wiel, *Catal. Today* 98 (2004) 575.
- [15] M.M. Doheim, S.A. Hanafy, G.A. El-Shobaky, *Mater. Lett.* 55 (2002) 304.
- [16] H. Idriss, E.G. Seebauer, *J. Mol. Catal. A: Chem.* 152 (2000) 201.
- [17] F. Aupretre, C. Descorme, D. Duprez, *Stud. Surf. Sci. Catal.* 145 (2003) 303.
- [18] T. Nishiguchi, T. Matsumoto, H. Kanai, K. Utani, Y. Matsumura, W.-J. Shen, S. Imamura, *Appl. Catal. A* 279 (2005) 273.
- [19] C. Diagne, H. Idriss, A. Kiennemann, *Catal. Commun.* 3 (2002) 565.
- [20] C. Diagne, H. Idriss, K. Pearson, M.A. Gomez-Garcia, A. Kiennemann, C.R. Acad. Sci. Chim. 7 (2004) 617.
- [21] T. Montini, L. De Rogatis, V. Gombac, P. Fornasiero, M. Graziani, *Appl. Catal. B* 71 (2007) 125.
- [22] H.S. Roh, Y. Wang, D.L. King, A. Platon, Y.H. Chin, *Catal. Lett.* 108 (2006) 15.
- [23] D. Srinivas, C.V.V. Satyanarayana, H.S. Potdar, P. Ratnasamy, *Appl. Catal. A* 246 (2003) 323.
- [24] J.P. Breen, R. Burch, H.M. Coleman, *Appl. Catal. B* 39 (2002) 65.
- [25] M.A. Vannice, *J. Catal.* 37 (1975) 449.
- [26] T. Iizuka, Y. Tanaka, K. Tanabe, *J. Catal.* 76 (1982) 1.
- [27] A. Boffa, C. Lin, A.T. Bell, G.A. Somorjai, *J. Catal.* 149 (1994) 149.
- [28] B. Jenewein, M. Fuchs, K. Hayek, *Surf. Sci.* 532 (2003) 364.
- [29] D. Martin, D. Duprez, *J. Mol. Catal.* 118 (1997) 113.
- [30] S. Bernal, J.J. Calvino, G.A. Cifredo, A. Laachir, V. Perrichon, J.M. Herrmann, *Langmuir* 10 (1994) 717.
- [31] D. Stull, E.F. Westrum Jr., G.C. Sinke, *The Chemical Thermodynamics of Organic Compounds*, R. E. Krieger Pub. Co., 1987.
- [32] Y. Madier, C. Descorme, A.M. Le Govic, D. Duprez, *J. Phys. Chem. B* 103 (1999) 10999.
- [33] M.G. Cutrufello, I. Ferino, V. Solinas, A. Primavera, A. Trovarelli, A. Auroux, C. Picciau, *Phys. Chem. Chem. Phys.* 1 (1999) 3369.
- [34] D.C. Grenoble, M.M. Estadt, D.F. Ollis, *J. Catal.* 67 (1981) 90.
- [35] J. Barbier Jr., D. Duprez, *Appl. Catal. B* 3 (1993) 61.
- [36] A. Trovarelli, *Catal. Rev. Sci. Eng.* 38 (1996) 439.
- [37] T. Shido, A. Yamaguchi, K. Asakura, Y. Iwasawa, *J. Mol. Catal. A* 163 (2000) 67.
- [38] H.-S. Roh, A. Platon, Y. Wang, D.L. King, *Catal. Lett.* 110 (2006) 1.
- [39] S. Cavallaro, *Energy Fuel* 14 (2000) 1195.
- [40] S. Cavallaro, V. Chiodo, A. Vita, S. Freni, *J. Power Sources* 123 (2003) 10.
- [41] G.A. Mills, F.W. Steffen, *Catal. Rev.* 8 (1973) 159.
- [42] M. Araki, V. Ponec, *J. Catal.* 44 (1976) 439.
- [43] J.A. Rabo, A.P. Risch, M.L. Poutsma, *J. Catal.* 53 (1978) 295.
- [44] J.G. McCarty, H. Wise, *J. Catal.* 57 (1979) 406.
- [45] J.L. Falconer, A.E. Zagli, *J. Catal.* 62 (1980) 280.
- [46] F. Solymosi, A. Erdöhelyi, T. Bansagi, *J. Catal.* 68 (1981) 371.
- [47] A. Trovarelli, C. de Leitenburg, G. Dolcetti, J.L. Lorca, *J. Catal.* 151 (1995) 111.
- [48] H. Kusama, K. Kitamura Bando, K. Okabe, H. Arakawa, *Appl. Catal. A* 197 (2000) 255.
- [49] A. Goguet, F. Meunier, J.P. Breen, R. Burch, M.I. Petch, A. Faur Ghenciu, *J. Catal.* 226 (2004) 382.